Journal of Sound and Vibration (2002) **249**(3), 483–498
doi:10.1006/jsvi.2001.3866, available online at http://www.idealibrary.com on IDEAL®

DYNAMIC RESPONSE OF TWO ROTORS CONNECTED BY RIGID MECHANICAL COUPLING WITH PARALLEL MISALIGNMENT

K. M. Al-Hussain and I. Redmond

Dynamic Analysis Unit, Saudi Aramco, E-7180, Dhahran 31311, P.O. Box 2535, Saudi Arabia.
E-mail: hussaikm@aramco.com.sa

(*Received* 15 *December* 2000, *and in final form* 21 *May* 2001)

The effect of parallel misalignment on the lateral and torsional responses of two rotating shafts (Jeffcott rotors) is examined with theoretical and numerical analysis. The general equations of motion are derived and given in dimensionless form to represent the general case. The equations of motion revealed that parallel misalignment couples the translation and angular deflections through the stiffness matrix and the force vector. The non-linear equations are solved numerically using a combination of Newmark and Newton–Raphson methods to determine the dimensionless frequency and transient responses in terms of misalignment magnitude. The numerical results show that the system natural frequencies are excited at transient condition due to the presence of pure parallel misalignment. At steady state condition, the $1\times$-rotational speed excitation is present in the translation and angular directions, which indicates that parallel misalignment can be a source of both torsional and lateral excitations.

1. INTRODUCTION

The problem of misalignment encountered in rotating machinery is of great concern to designers and maintenance engineers. The need for understanding the phenomena is important to practical engineers for the purpose of trouble shooting. Most rotating machinery consists of a driver and a driven machine, which are coupled through some type of coupling. There are many types of industrial couplings some of which are of rigid, gear, and flexible type. The couplings' function is to transmit torque from the driver to the driven machine. There are two types of coupling misalignments: parallel and angular. A combination of parallel and angular misalignment is common in the industry. This causes high vibrations with different symptoms that sometimes cannot be explained. There are a lot of discussions in the industry regarding the interpretation of the vibration signal, caused by misalignment, coming from a machine, but there is not enough academic research that explains the phenomena in a simple way.

According to Lorenzen *et al.* [1], for many decades, it has been common to use solid couplings in turbomachinery; however, these couplings have a decisive influence on rotordynamics. Reference [1] introduced a comparison of critical speeds of a high-speed/high-power compressor train alternatively equipped with solid couplings, flexible-disc, or gear-type couplings. In reference [1], the imbalance response using different types of couplings was calculated for comparison purposes, which led to the conclusion that solid couplings can cause the rotor to be more stable. Sekhar and Prabhu [2] presented the effects of coupling misalignment on turbomachinery vibrations. It was shown that the

0022-460X/02/030483 + 16 $35.00/0

location of the coupling with respect to the bending mode shape has a strong influence on the level of vibration. A theoretical model of a complete motor–flexible coupling rotor was presented by Xu and Marangoni [3, 4]. They assumed that the flexible coupling behaves exactly as a universal joint to take the misalignment effect into account. An experimental investigation on the misalignment effect on cylindrical and three-lobe journal bearings was conducted by Prabhu [5]. Reference [5] showed that an increase in angular misalignment had caused change in the second harmonic of the vibration response. Simon [6] predicted the behavior of large turbo-machinery when subjected to imbalance and misalignment. The vibration excited by the coupling was computed numerically using assumed values for the reaction forces and moments at the coupling. Dewell and Mithchell [7] developed the expected vibration frequencies for a misaligned metallic disk-flexible coupling. The predicted dominant frequencies were $2\times$ and $4\times$ running speed components due to angular misalignment.

Wattner [8] has dealt with the design functions and case histories of gear couplings. He discussed the various types of misalignments, which may be encountered by the gear type of coupling. Case histories were presented in reference [8] for different types of coupling failures. Forces and moments, induced by gear coupling misalignment, were addressed by Palazzolo *et al.* [9]. Palazzolo *et al.* addressed the fact that gear couplings can produce large static forces that can affect the vibration of turbomachinery. Bloch [10] has shown how a change from conventional gear-type couplings to more recent diaphram coupling design can lower shaft stresses sufficiently to avoid shaft replacement during power uprates of centrifugal compressors. The reaction forces generated by the different types of couplings were derived by Gibbson [11]. The applications of flexible-type couplings for turbomachinery were discussed by Mancuso [12]. This reference includes reasons for using flexible couplings, difference between gear and flexible element couplings, and selection of coupling for new applications.

Rosenberg [13] presented the critical speed behavior of rotating shafts driven by universal coupling. It has been shown in reference [13] that the models can develop mild instabilities at odd-ordered integer submultiples of the critical speed. Saigo *et al.* [14] investigated the instability of a rotor system induced by Coulomb friction in universal joints theoretically and experimentally. Reducing the friction leads to substantial reduction in the destabilizing forces. Sheu *et al.* [15] examined the effects of joint angles and joint friction on the steady state responses of a double universal joint system. It has been discovered that the misalignment angles have a great effect on fluctuation in the output speed. Lateral and torsional vibration coupling in rotating machinery commonly refer to gear set. Hudson [16] has shown that a serious radial gear vibration was determined to be due to significant torsional excitation. His field test data verified and quantified that the frequency and magnitude of the torque was due to non-synchronous distortion. Means of controlling the torsional vibration of synchronous motor-driven compressors was introduced by Al-Bedoor *et al.* [17]. In reference [17], a dual dynamic absorber was used in the model in an attempt to reduce the torsional excitation. The result of this study showed that this kind of torsional absorber can contribute to solving practical problems. Mancuso *et al.* [18] have made a comparison between general- and special-purpose couplings. Three basic functions of a flexible-type coupling are transmitted power, misalignment and end movement.

To this end, one can summarize that few studies have covered the detailed approach of analyzing parallel misalignment and its effect on the lateral and torsional responses. Some of these studies suffer from a modelling point of view to represent misalignment in its simplest form able to be understood by the practical engineer. Moreover, little attention was given to torsional excitation due to parallel misalignment. To the knowledge of the authors, no study has discussed the lateral and torsional coupling due to pure parallel misalignment.

The present work is devoted toward the analysis of a rigid coupling model, exposed to parallel misalignment, to aid turbomachinery diagnostic engineers in the understanding of the dynamic response of a misaligned system. The work starts by developing the equations of motions of two machines whose axis of rotation is offset due to pure parallel misalignment. The equations of motion are set in dimensionless form for numerical analysis to study the general effect of misalignment on the lateral and torsional responses. A combination of Newmark beta and Newton–Raphson algorithms is used to solve the resulting dimensionless non-linear equations of motion. Dimensionless frequency response is also derived and solved numerically to aid the practical engineer to distinguish between unbalanced, bowed and misaligned responses. This work can be extended to include angular and combined misalignment by using co-ordinate transformation, which will be presented in future work.

2. THE DYNAMIC MODEL

2.1. SYSTEM DESCRIPTIONS AND ASSUMPTIONS

Two disks are mounted at the center of two flexible rotors and connected through a rigid mechanical coupling. The two shafts are in parallel misalignment state of magnitude δ as shown in Figure 1. The two shafts have the mass centers of the two disks displaced distances e_1 and e_2 from the shafts' centerlines. Assuming that the disks are rotating in their own planes, no gyroscopic effects are included in the model. Both disks 1 and 2 rotate with variable angular velocity, $\dot{\beta}_1$ and $\dot{\beta}_2$.

For simplification purposes, it is assumed that the two shafts axes are misaligned initially in the x direction. Instantaneous positions of the two disks and the coupling are shown in Figure 2.

2.2. KINETIC AND POTENTIAL ENERGIES EXPRESSIONS

The generalized co-ordinate for the system is

$$\{q\} = [x_1, y_1, \beta_1, x_2, y_2, \beta_2]. \tag{1}$$

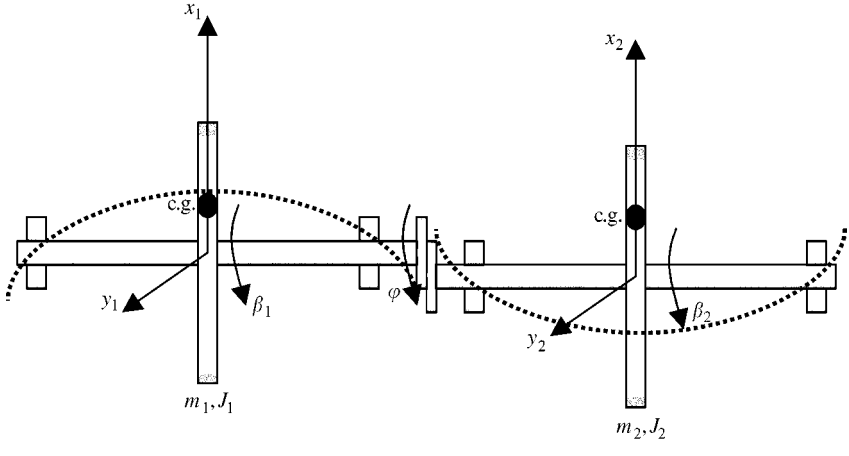

Figure 1. Two masses flexible rotors in a parallel misalignment state.

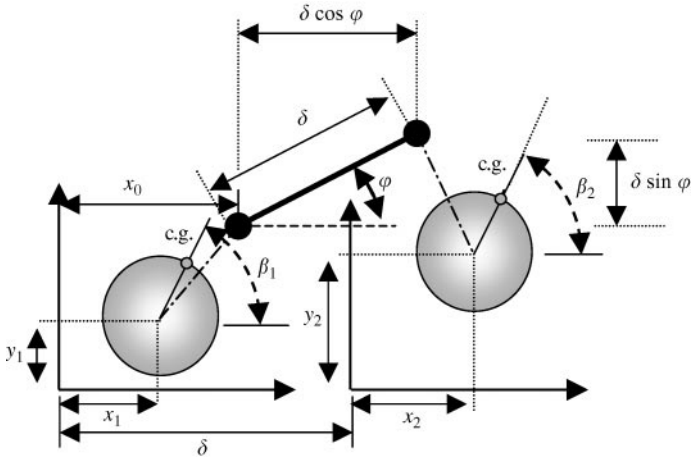

Figure 2.. Instantaneous locations of the two disks and coupling.

The total kinetic energy is constituted of driver kinetic energy and the driven kinetic energy. The system kinetic energy can be written as

$$T = \frac{1}{2}m_1[(\dot{x}_1 - e_1\dot{\beta}_1 \sin\beta_1)]^2 + \frac{1}{2}m_1[(\dot{y}_1 + e_1\dot{\beta}_1 \cos\beta_1)]^2 + \frac{1}{2}m_2[(\dot{x}_2 - e_2\dot{\beta}_2 \sin\beta_2)]^2$$

$$+ \frac{1}{2}m_2[(\dot{y}_2 + e_2\dot{\beta}_2 \cos\beta_2)]^2 + \frac{1}{2}J_1\dot{\beta}_1^2 + \frac{1}{2}J_2\dot{\beta}_2^2. \tag{2}$$

The potential energy is

$$V = \frac{1}{2}k_1x_1^2 + \frac{1}{2}k_1y_1^2 + \frac{1}{2}k_1'(x_1 - x_a)^2 + \frac{1}{2}k_1'(y_1 - y_a)^2 + \frac{1}{2}k_{t1}(\beta_1 - \varphi)^2$$

$$+ \frac{1}{2}k_2x_2^2 + \frac{1}{2}k_2y_2^2 + \frac{1}{2}k_2'(x_a + \delta\cos\varphi - x_2 + \delta)^2 + \frac{1}{2}k_2'(y_a + \delta\sin\varphi - y_2)^2$$

$$+ \frac{1}{2}k_{t2}(\varphi - \beta_2)^2 + m_1\mathbf{g}(y_1 + e_1\sin\beta_1) + m_2\mathbf{g}(y_2 + e_2\sin\beta_2). \tag{3}$$

The parallel misalignment magnitude appears in the potential energy equation only, which is an indication that it will appear in the system stiffness matrix.

2.3. THE EQUATIONS OF MOTION

Upon substituting the kinetic and potential energy expressions into the Lagrange equation, performing partial differentiation and manipulation, the system equation of motion is found as

$$[m]\{\ddot{q}\} + [k]\{q\} = \{F\}. \tag{4}$$

where the mass matrix is

$$[m] = \begin{bmatrix} m_1 & 0 & -m_1 e_1 \sin\beta_1 & 0 & 0 & 0 \\ 0 & m_1 & m_1 e_1 \cos\beta_1 & 0 & 0 & 0 \\ -m_1 e_1 \sin\beta_1 & m_1 e_1 \cos\beta_1 & J_1 + m_1 e_1^2 & 0 & 0 & 0 \\ 0 & 0 & 0 & m_2 & 0 & -m_2 e_2 \sin\beta_2 \\ 0 & 0 & 0 & 0 & m_2 & m_2 e_2 \cos\beta_2 \\ 0 & 0 & 0 & -m_2 e_2 \sin\beta_2 & m_2 e_2 \cos\beta_2 & J_2 + m_2 e_2^2 \end{bmatrix}. \tag{5}$$

The stiffness matrix is

$$[k] = \begin{bmatrix} \frac{k_1 k_1' + 2k_1' k_2'}{k_1' + k_2'} & 0 & 0 & -\frac{k_1' k_2'}{k_1' + k_2'} & 0 & 0 \\ 0 & \frac{k_1 k_1' + 2k_1' k_2'}{k_1' + k_2'} & 0 & 0 & -\frac{k_1' k_2'}{k_1' + k_2'} & 0 \\ -\frac{k_1' k_2' k_{t1} \delta \sin\varphi}{(k_1' + k_2')(k_{t1} + k_{t2})} & \frac{k_1' k_2' k_{t1} \delta \cos\varphi}{(k_1' + k_2')(k_{t1} + k_{t2})} & \frac{k_{t1} k_{t2}}{k_{t1} + k_{t2}} & \frac{k_{t1} k_1' k_2' \delta \sin\varphi}{(k_{t1} + k_{t2})(k_1' + k_2')} & -\frac{k_{t1} k_1' k_2' \delta \cos\varphi}{(k_{t1} + k_{t2})(k_1' + k_2')} & -\frac{k_{t1} k_{t2}}{k_{t1} + k_{t2}} \\ \frac{-k_1' k_2'}{k_1' + k_2'} & 0 & 0 & \frac{k_2 k_2' + 2k_1 k_2}{k_1' + k_2'} & 0 & 0 \\ 0 & -\frac{k_1' k_2'}{k_1' + k_2'} & 0 & 0 & \frac{k_2 k_2' + 2k_1' k_2'}{k_1' + k_2'} & 0 \\ -\frac{k_1' k_2' k_{t2} \delta \sin\varphi}{(k_1' + k_2')(k_{t1} + k_{t2})} & \frac{k_1' k_2' k_{t2} \delta \cos\varphi}{(k_1' + k_2')(k_{t1} + k_{t2})} & -\frac{k_{t1} k_{t2}}{k_{t1} + k_{t2}} & \frac{k_{t2} k_1' k_2' \delta \sin\varphi}{(k_{t1} + k_{t2})(k_1' + k_2')} & -\frac{k_{t2} k_1' k_2' \delta \cos\varphi}{(k_{t1} + k_{t2})(k_1' + k_2')} & \frac{k_{t2} k_{t1}}{k_{t1} + k_{t2}} \end{bmatrix}. \tag{6}$$

$$\{F\} = \begin{Bmatrix} m_1 e_1 \dot\beta_1^2 \cos\beta_1 - (k_1' k_2')/(k_1' + k_2')\,\delta \cos\varphi + (k_1' k_2'/(k_1' + k_2'))\,\delta \\ m_1 e_1 \dot\beta_1^2 \sin\beta_1 - (k_1' k_2')/(k_1' + k_2')\,\delta \sin\varphi - m\mathbf{g} \\ T(t) - m_1 \mathbf{g} e_1 \cos\beta_1 \\ m_2 e_2 \dot\beta_2^2 \cos\beta_2 + (k_1' k_2')/(k_1' + k_2')\,\delta \cos\varphi - (k_1' k_2')/(k_1' + k_2')\,\delta \\ m_2 e_2 \dot\beta_2^2 \sin\beta_2 + (k_1' k_2')/(k_1' + k_2')\,\delta \sin\varphi - m\mathbf{g} \\ -T_L(t) - m_2 \mathbf{g} e_2 \cos\beta_2 \end{Bmatrix}. \tag{7}$$

The angle φ is the coupling angular position, which is a function of all co-ordinates.

$$\varphi = \frac{k_{t1}}{k_{t1} + k_{t2}}\beta_1 + \frac{k_{t2}}{k_{t1} + k_{t2}}\beta_2 + \frac{k_1' k_2'}{(k_{t1} + k_{t2})(k_1' + k_2')} \times \delta\,[x_1 \sin\varphi - x_2 \sin\varphi - y_1 \cos\varphi + y_2 \cos\varphi]. \tag{8}$$

The equations describing the coupling end positions are

$$x_a = (k'_1/(k'_1 + k'_2))\, x_1 + (k'_2/(k'_1 + k'_2))\, x_2 - (k'_2/(k'_1 + k'_2))\, \delta \cos\varphi + (k'_2/k'_1 + k'_2))\, \delta, \quad (9)$$

$$y_a = (k'_1/(k'_1 + k'_2))\, y_1 + (k'_2/(k'_1 + k'_2))\, y_2 - (k'_2/(k'_1 + k'_2))\, \delta \sin\varphi. \quad (10)$$

The mass matrix equation (5) shows that the lateral and torsional equations are coupled due to the imbalance effect of disks' eccentricities e_1 and e_2. Alignment has no effect on the inertial forces. The stiffness matrix equation (6) shows that misalignment couples the angular motion to the translation motions. Misalignment influence on the lateral motion appears in the force vector equation (7). Due to the assumption that misalignment is present initially in the x direction, there is a preload term appearing in the x direction as in equation (7). The coupling angular position φ, equation (8), is a non-linear function of all spatial co-ordinates and a function of the misalignment magnitude. The coupling motion can be described by equations (9) and (10), which are functions of the lateral positions of both disks and a function of the misalignment magnitude.

2.4. EQUATIONS OF MOTION IN NON-DIMENSIONAL FORM

The following parameters are introduced to simplify the equations:

$$k'_e = (k'_1 k'_2/(k'_1 + k'_2)), \quad k_{te} = (k_{t1} k_{t2}/(k_{t1} + k_{t2}), \quad \omega_{n1}^2 = k'_e/m_1, \quad \omega_{n2}^2 = k'_e/m_2. \quad (11\text{–}14)$$

The equation of motion (4) can be written in dimensionless form by dividing the equations of motion by $k'_e \delta$, factoring $1/\delta$ into the logitudinal space vectors, which will make all displacement vectors dimensionless, introducing a dimensionless time $t^* = \omega_{n1} t$, and dividing the torsional equations by δ.

By introducing the dimensionless space vector

$$\{q^*\} = \{x_1/\delta, y_1/\delta, \beta_1, x_2/\delta, y_2/\delta, \beta_2\}^{\mathrm{T}} = \{x_1^*, y_1^*, \beta_1, x_2^*, y_2^*, \beta_2\}^{\mathrm{T}}, \quad (15)$$

the equations of motion reduce to

$$[m^*]\{\ddot{q}^*\} + [c^*]\{\dot{q}^*\} + [k]\{q^*\} = \{F^*\}. \quad (16)$$

where the dimensionless mass matrix is

$$[m^*] = \begin{bmatrix} 1 & 0 & -\frac{e_1}{\delta}\sin\beta_1 & 0 & 0 & 0 \\ 0 & 1 & \frac{e_1}{\delta}\cos\beta_1 & 0 & 0 & 0 \\ -\frac{e_1}{\delta}\sin\beta_1 & \frac{e_1}{\delta}\cos\beta_1 & \frac{J_1 + m_1 e_1^2}{\delta^2 m_1} & 0 & 0 & 0 \\ 0 & 0 & 0 & \frac{m_2}{m_1} & 0 & -\frac{e_2}{\delta}\frac{m_2}{m_1}\sin\beta_2 \\ 0 & 0 & 0 & 0 & \frac{m_2}{m_1} & \frac{e_2}{\delta}\frac{m_2}{m_1}\cos\beta_2 \\ 0 & 0 & 0 & -\frac{e_2}{\delta}\frac{m_2}{m_1}\sin\beta_2 & \frac{e_2}{\delta}\frac{m_2}{m_1}\cos\beta_2 & \frac{J_2 + m_2 e_2^2}{\delta^2 m_1} \end{bmatrix}. \quad (17)$$

To introduce low damping into the system, assume the damping matrix $[C] = \text{diag}[c]$. To introduce the damping factor into the equations of motion, it needs to be divided by $\delta k'_e$. Therefore, for simplicity, the damping element is assumed to be

$$c = 2\zeta m_1 \omega_{n1}/\delta k'_e \tag{18}$$

for the lateral degrees of freedom, where δ/ω_{n1} is factored into the velocity vector, reducing the damping element to $c = 2\zeta$. For the torsional degrees of freedom assume

$$c_t = 2\zeta J_1 \omega_{nt}/\delta^2 k'_e. \tag{19}$$

where $1/\omega_{n1}$ is factored into the angular velocity vector producing the dimensionless damping matrix

$$[c^*] = \begin{bmatrix} 2\zeta & 0 & 0 & 0 & 0 & 0 \\ 0 & 2\zeta & 0 & 0 & 0 & 0 \\ 0 & 0 & 2\zeta & 0 & 0 & 0 \\ 0 & 0 & 0 & 2\zeta & 0 & 0 \\ 0 & 0 & 0 & 0 & 2\zeta & 0 \\ 0 & 0 & 0 & 0 & 0 & 2\zeta \end{bmatrix}. \tag{20}$$

The dimensionless stiffness matrix is

$$[k^*] = \begin{bmatrix} k_1/k'_2 + 2 & 0 & 0 & -1 & 0 & 0 \\ 0 & k_1/k'_2 + 2 & 0 & 0 & -1 & 0 \\ -(k_{te}/k_{t2})\sin\varphi & (k_{te}/k_{t2})\cos\varphi & k_{te}/\delta^2 k'_e & (k_{te}/k_{t2})\sin\varphi & -(k_{te}/k_{t2})\cos\varphi & -k_{te}/\delta^2 k'_e \\ -1 & 0 & 0 & k_2/k'_1 + 2 & 0 & 0 \\ 0 & -1 & 0 & 0 & k_2/k'_1 + 2 & 0 \\ -(k_{te}/k_{t1})\sin\varphi & k_{te}/k_{t1}\cos\varphi & -(k_{te}/\delta^2 k'_e) & (k_{te}/k_{t1})\sin\varphi & -(k_{te}/k_{t1})\cos\varphi & k_{te}/\delta^2 k'_e \end{bmatrix}. \tag{21}$$

The dimensionless force vector is

$$\{F^*\} = \begin{Bmatrix} (1/\omega_{n1}^2)\, e_1/\delta\, \dot\beta_1^2 \cos\beta_1 - \cos\varphi + 1 \\ (1/\omega_{n1}^2)\, e_1/\delta\, \dot\beta_1^2 \sin\beta_1 - \sin\varphi - (1/\omega_{n1}^2)(\mathbf{g}/\delta) \\ T(t)/\delta^2 k'_e - (1/\omega_{n1}^2)\mathbf{g}(e_1/\delta)\cos\beta_1 \\ (1/\omega_{n2}^2)(e_2/\delta)\,\dot\beta_2^2 \cos\beta_2 + \cos\varphi - 1 \\ (1/\omega_{n2}^2)(e_2/\delta)\,\dot\beta_2^2 \sin\beta_2 + \sin\varphi - (1/\omega_{n2}^2)\,\mathbf{g}/\delta \\ -(T_L(t)/(\delta^2 k'_e) - (1/\omega_{n2}^2)\,\mathbf{g}(e_2/\delta)\cos\beta_2 \end{Bmatrix} \tag{22}$$

The coupling angular position in terms of the dimensionless co-ordinates is

$$\varphi = (k_{te}/k_{t1})\beta_1 + (k_{te}/k_{t2})\beta_2 + (k_{te}\delta^2/(k_{t1} + k_{t2}))\,[(x_1^* - x_2^*)\sin\varphi - (y_1^* - y_2^*)\cos\varphi]. \tag{23}$$

The equations that describe the coupling lateral deflections are

$$x_a^* = (k'_e/k'_2)\, x_1^* + (k'_e/k'_1)\, x_2^* - (k'_e/k'_1)\cos\varphi + k'_2/(k'_1 + k'_2). \tag{24}$$

$$y_a^* = (k'_e/k'_2)\, y_1^* + (k'_e/k'_1)\, y_1^* - (k'_e/k'_{12})\sin\varphi. \tag{25}$$

2.5. FREQUENCY RESPONSE OF THE MISALIGNED SHAFTS—AMPLITUDE AND PHASE ANGLE

To examine the lateral frequency response of the system, the torsional degrees of freedom are removed from the system. Assume constant angular velocity ω of the whole assembly. Set the imbalance phase angles to ϕ_{u1} and ϕ_{u2}, for disks 1 and 2 respectively. The misalignment initial phase angle is defined by ϕ_m, The dimensionless frequency response equation is

$$\{q^*\} = \{x_1^*, y_1^*, x_2^*, y_2^*\}^{\mathrm{T}}. \tag{26}$$

$$\begin{bmatrix} 1 & 0 & 0 & 0 \\ 0 & 1 & 0 & 0 \\ 0 & 0 & m_2/m_1 & 0 \\ 0 & 0 & 0 & m_2/m_1 \end{bmatrix} \begin{Bmatrix} \ddot{x}_1^* \\ \ddot{y}_1^* \\ \ddot{x}_2^* \\ \ddot{y}_2^* \end{Bmatrix} + \begin{bmatrix} 2\zeta & 0 & 0 & 0 \\ 0 & 2\zeta & 0 & 0 \\ 0 & 0 & 2\zeta & 0 \\ 0 & 0 & 0 & 2\zeta \end{bmatrix} \begin{Bmatrix} \dot{x}_1^* \\ \dot{y}_1^* \\ \dot{x}_2^* \\ \dot{y}_2^* \end{Bmatrix}$$

$$+ \begin{bmatrix} k_1/k_2' + 2 & 0 & -1 & 0 \\ 0 & k_1/k_2' + 2 & 0 & -1 \\ -1 & 0 & k_2/k_1' + 2 & 0 \\ 0 & -1 & 0 & k_2/k_1' + 2 \end{bmatrix} \begin{Bmatrix} x_1^* \\ y_1^* \\ x_2^* \\ y_2^* \end{Bmatrix}$$

$$= \begin{Bmatrix} (e_1/\delta)(\omega/\omega_{n1})^2 \cos(\omega/\omega_{n1}\, t^* + \phi_{u1}) - \cos(\omega/\omega_{n1}\, t^* + \phi_m) + \cos\phi_m \\ (e_1/\delta)(\omega/\omega_{n1})^2 \sin(\omega/\omega_{n1}\, t^* + \phi_{u1}) - \sin(\omega/\omega_{n1}\, t^* + \phi_m) + \sin(\phi_m) \\ (e_2/\delta)(\omega/\omega_{n1})^2 \cos(\omega/\omega_{n1}\, t^* + \phi_{u2}) + \cos(\omega/\omega_{n1}\, t^* + \phi_m) - \cos\phi_m \\ (e_2/\delta)(\omega/\omega_{n1})^2 \sin(\omega/\omega_{n1}\, t^* + \phi_{u2}) + \sin(\omega/\omega_{n1}\, t^* + \phi_m) - \sin(\phi_m) \end{Bmatrix}. \tag{27}$$

Transforming the above equation into the complex domain by setting

$$z_1^* = x_1^* + \mathrm{i}y_1^*, \quad z_2^* = x_2^* + \mathrm{i}y_2^*. \tag{28, 29}$$

the dimensionless frequency response equation in complex form is

$$\begin{bmatrix} 1 & 0 \\ 0 & m_2/m_1 \end{bmatrix} \begin{Bmatrix} \ddot{z}_1^* \\ \ddot{z}_1^* \end{Bmatrix} + \begin{bmatrix} 2\zeta & 0 \\ 0 & 2\zeta \end{bmatrix} \begin{Bmatrix} \dot{z}_1^* \\ \dot{z}_1^* \end{Bmatrix} + \begin{bmatrix} k_1/k_2' + 2 & -1 \\ -1 & k_2/k_1' + 2 \end{bmatrix} \begin{Bmatrix} z_1^* \\ z_1^* \end{Bmatrix}$$

$$= \begin{Bmatrix} (e_1/\delta) f_{n1}^2\, \mathrm{e}^{\mathrm{i}(f_{n1}t^* + \phi_{u1})} - \mathrm{e}^{\mathrm{i}(f_{n1}t^* + \phi_m)} + \mathrm{e}^{\mathrm{i}(\phi_m)} \\ (e_2/\delta) f_{n1}^2\, \mathrm{e}^{\mathrm{i}(f_{n1}t^* + \phi_{u2})} + \mathrm{e}^{\mathrm{i}(\omega t + \phi_m)} - e^{\mathrm{i}(\phi_m)} \end{Bmatrix} \tag{30}$$

where

$$f_{n1} = \omega/\omega_{n1}. \tag{31}$$

For constant velocity, assume the solution of the form

$$\{z^*\} = \{z_0^*\} + \{z_r^*\}\, \mathrm{e}^{\mathrm{i}f_{n1}t^*}. \tag{32}$$

$$\{z^*\} = [[k] - f_{n1}[m] + \mathrm{i}f_{n1}[c]]^{-1} \begin{Bmatrix} (e_1/\delta) f_{n1}^2\, \mathrm{e}^{\mathrm{i}\phi_{u1}} - \mathrm{e}^{\mathrm{i}\phi_m} \\ (e_2/\delta) f_{n1}^2\, \mathrm{e}^{\mathrm{i}\phi_{u2}} + \mathrm{e}^{\mathrm{i}\phi_m} \end{Bmatrix} + [k]^{-1} \begin{Bmatrix} \mathrm{e}^{\mathrm{i}\phi_m} \\ -\mathrm{e}^{\mathrm{i}\phi_m} \end{Bmatrix}. \tag{33}$$

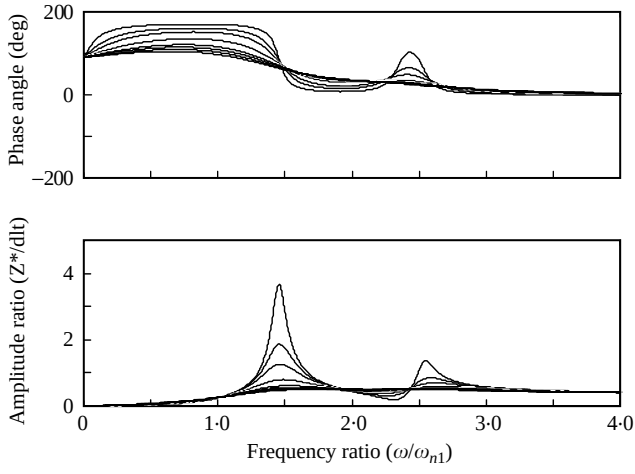

Figure 3. Disk 1 dimensionless response due to parallel misalignment versus frequency ratio.

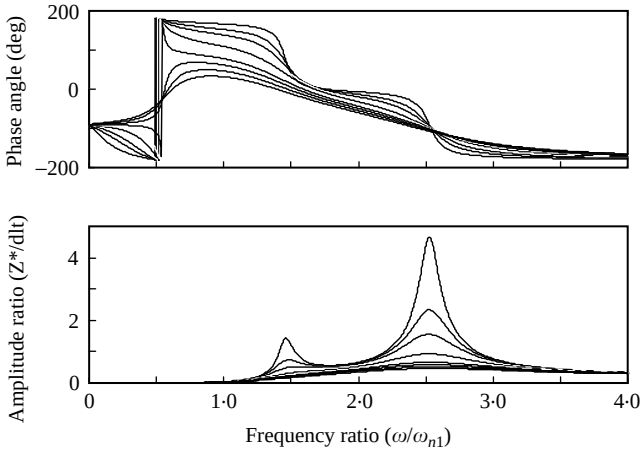

Figure 4.. Disk 2 dimensionless response due to parallel misalignment versus frequency ratio.

This describes the system amplitude of motion of the steady state circular synchronous precession.

3. NUMERICAL ANALYSIS

3.1. DIMENSIONLESS FREQUENCY RESPONSES

The dynamic response and phase angle for two Jeffcott rotors on flexible supports due to parallel misalignment, and combined parallel misalignment and imbalance can be calculated using equation (33). Equation (33) is in dimensionless form with respect to the misalignment magnitude, δ.

The frequency responses due to pure parallel misalignment are shown in Figures 3, 4, and 5 for rotor 1, rotor 2, and the coupling respectively. These curves correspond to the rotor amplitudes and phase angles for the values of damping ratios varying from 0·05 to

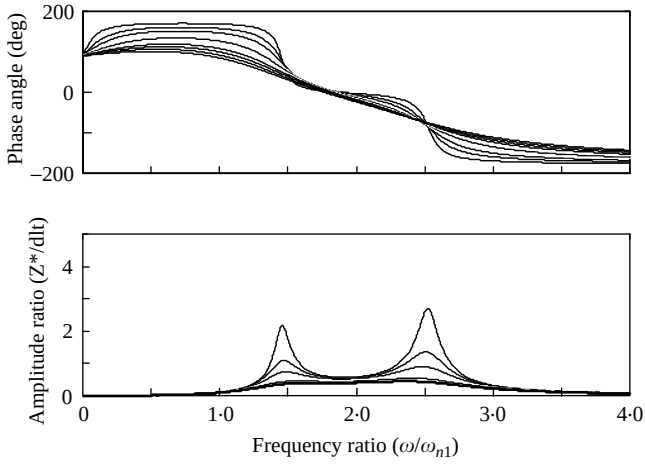

Figure 5. Coupling dimensionless response due to parallel misalignment versus frequency ratio.

0·15, with steps of 0·01. The system parameters selected to generate these plots are estimated from the basis of selected model values in which both lateral natural frequencies are excited. The chosen parameter values are $m_2/m_1 = \frac{2}{3}$, $k_1/k_2' = \frac{1}{2}$, $k_2/k_1' = 2$, and the initial misalignment angle is $\phi_m = 0$.

For the selected parameters both natural frequencies (1·5 and 2·5) are excited by the parallel misalignment. It can be seen that as the damping decreases, both amplitudes change significantly, as expected. The effect of residual shaft bow on imbalance response is presented in detail in reference [19]. A similar approach can be applied to equation (33) to study the effect of parallel misalignment on imbalanced rotors for different angles.

3.2. TRANSIENT ANALYSIS

Transient response is calculated by solving the non-linear dimensionless equations of motion (16 and 23) using the Newmark beta and Newton–Raphson methods. Although the equations of motion are dimensionless, it is difficult to decide what are the realistic values for these parameters. Therefore, selection of these dimensionless parameters is based on a realistic model. The selected model parameters are $\delta = 254$ mm, $m_1 = 1{\cdot}2$ kg, $J_1 = 9{\cdot}6 \times 10^{-4}$ kg m^2, $e_1 = 0$, $k_1 = 2{\cdot}4 \times 10^5$, $k_{t1} = 291$ m N/rad, $m_2/m_1 = 1$, $k_2 = k_1 = k_1' = k_2'$ and $J_2/J_1 = \frac{1}{5}$.

Due to the non-linearity of the equations of motion, which are a function of the non-linear coupling angle φ, equations of motion are integrated numerically using Newmark beta, where the Newton–Raphson method is used to compute φ at each time step and checked for convergence. The Newmark beta parameters for accuracy and stability are selected as $\alpha = 0{\cdot}5$, $\beta = 0{\cdot}25$. The dimensionless time step is selected as $\Delta t^* = 0{\cdot}03$. The dimensionless initial conditions are $\{q_0^*\} = \{0\}$, $\{\dot{q}_0^*\} = \{0\}$, $\{\ddot{q}_0^*\} = [m]^{-1}\{T_0^*\}$ and $\varphi = 0$ at $t^* = 0$. The dimensionless input torque, $T_i^* = 2000$ is assumed constant whilst the load torque is assumed to be proportional to the square of angular speed $T_L^* = \alpha \dot{\beta}_2^{*2}$, where, $\alpha = T_i^*/[36000(2\pi/60)/\omega_{n1}]^2$.

Figure 6 shows the dimensionless input, load torques, and the dimensionless speed curve. The maximum dimensionless speed reached is 11·91 in dimensionless time of 150. The

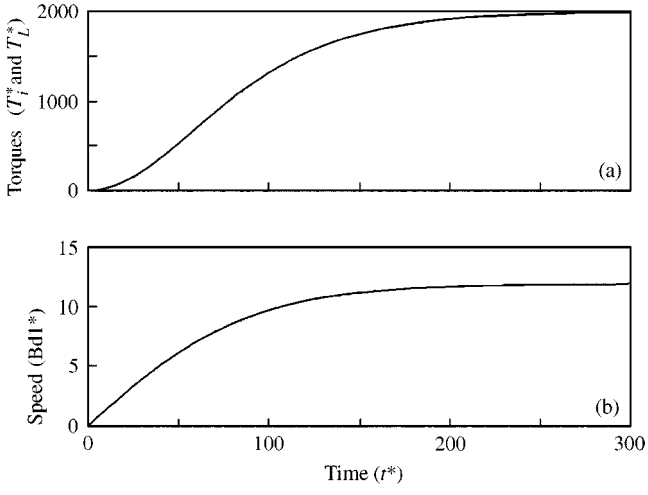

Figure 6. Dimensionless input and load torques (a) and the resultant speed; (b) versus time.

values of the input and the load torques are selected so the model natural frequencies are excited during the transient condition.

The dimensionless transient response of the disks 1 and 2 in the x direction is presented in Figure 7. The responses show that the lateral and torsional dimensionless natural frequencies (1·95 and 9·57) are excited due to pure parallel misalignment. The second lateral natural frequency (4·0) is not excited for the selected symmetrical parameters in the lateral direction, which puts the coupling at a nodal point. Both disks 1 and 2 start at zero position and move outward in the x direction (direction of misalignment). Both disks start at zero position due to the basic assumption in the derivation of equations, that when the two units are coupled there is no initial preload exerted across the coupling. Both shafts are at zero position while at rest, and they both take different static positions as soon as the input torque is applied.

Initially, both disks start at zero position and as soon as the input torque is applied both disks move outward taking a new static position, as shown in Figure 8. The new dimensionless static position is in the x direction, the direction of assumed misalignment. The initial orbits show that the rotors take opposite positions from each other.

The steady state orbits and time response for each rotor are shown in Figure 9. Due to the excitation of lateral natural frequencies for the chosen parameters, the orbits have five inner loops. These loops are due to the excitation of the lateral natural frequency at steady state condition. For the chosen parameters, the steady state frequency (11·33) is approximately 5·8 times the excited lateral natural (1·95) frequency. The final steady state static positions of the rotors 1 and 2 are 0·25 and $-0{\cdot}25$ respectively.

The steady state frequency contents of the waveforms are shown in Figure 10. Fast Fourier transform (FFT) with 1024 points and a sampling rate of 200 is applied to the time signal from $t^* = 240$ to $t^* = 300$. In Figure 10, the horizontal axis is the dimensionless frequency form, ω/ω_{n1}. The vertical axis is the logarithmic scale of the power spectral density of the steady-state waveform. The system's lateral and torsional dimensionless natural frequencies (1·95 and 9·57) are excited. The steady state dimensionless exciting frequency is 11·33. This frequency component appears in the lateral and torsional directions, which indicates that pure parallel misalignment can cause lateral–torsional excitations of the natural frequencies during normal operation of rotating machinery.

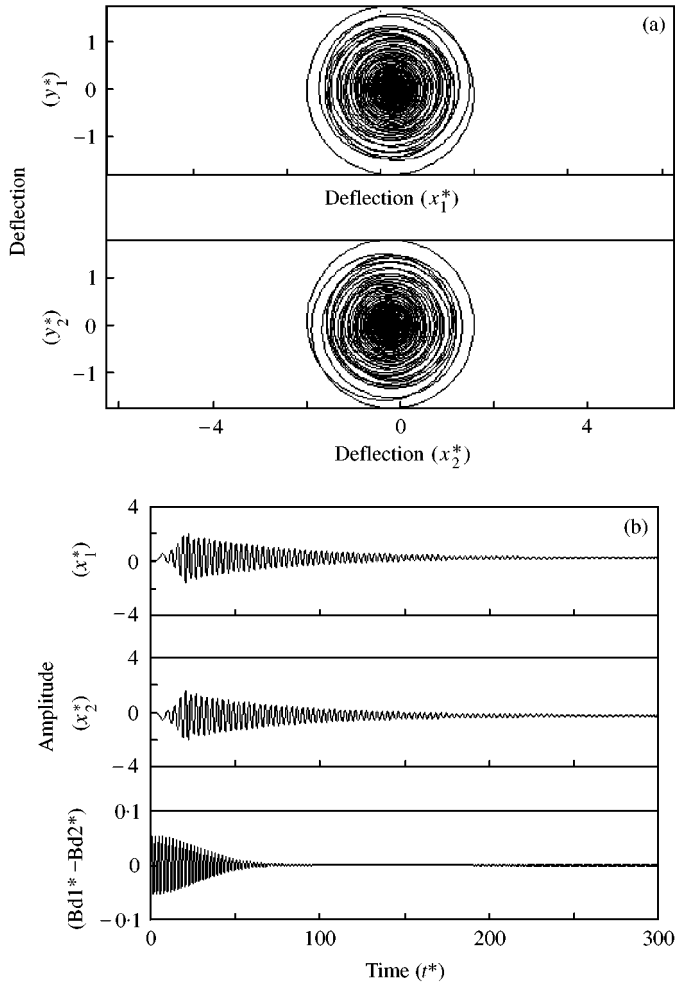

Figure 7. Rotor system response using the lateral–torsional model: (a) transient orbit; (b) dimensionless lateral and torsional response.

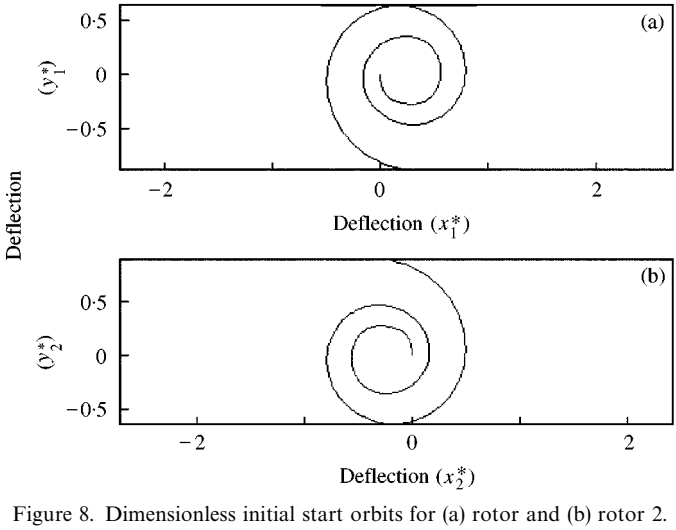

Figure 8. Dimensionless initial start orbits for (a) rotor and (b) rotor 2.

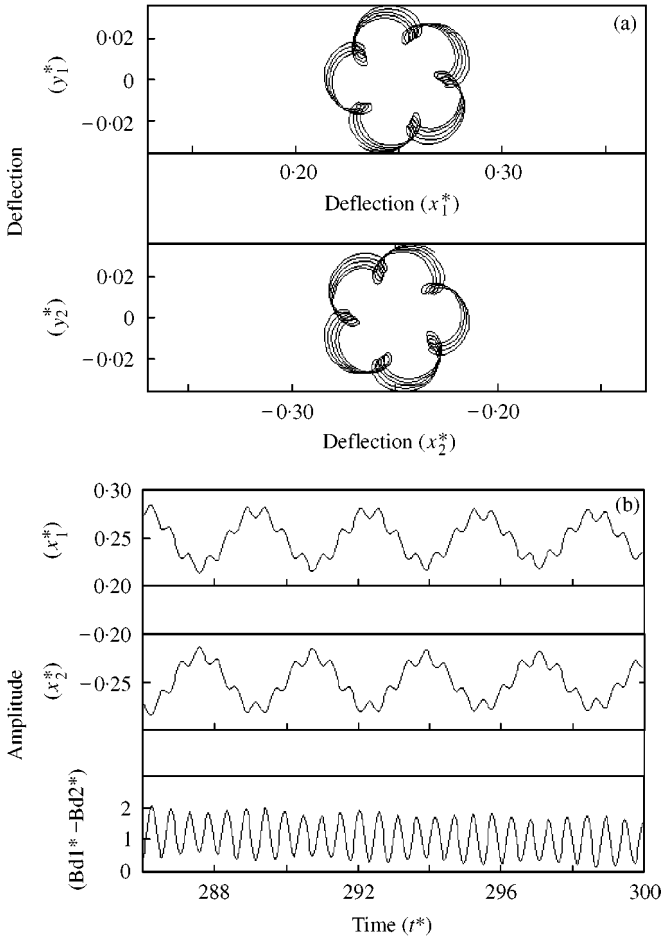

Figure 9. Steady state lateral–torsional model using the lateral torsional mode: (a) steady state orbits; (b) steady state response.

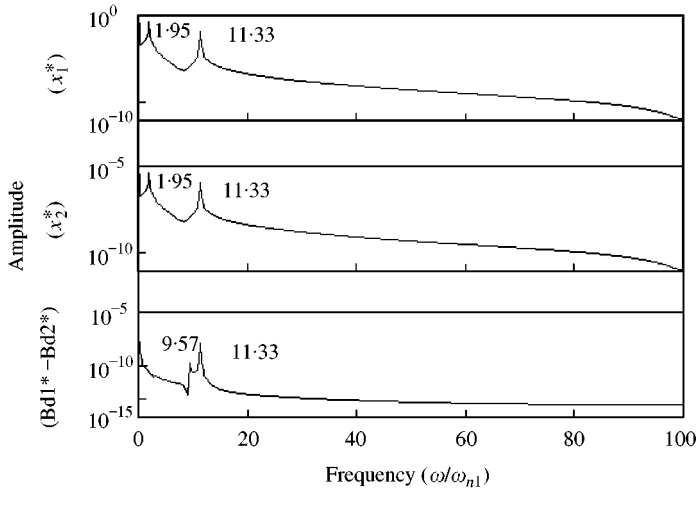

Figure 10. Dimensionless frequency responses.

4. CONCLUSION

In this study, a model for coupled lateral and torsional vibrations of two rotors subjected to pure parallel misalignment has been developed. The system degrees of freedom are the model's four orthogonal lateral deflections, the rigid-body rotation, and the model's torsional deformation. The system equations of motion are obtained using the Lagrange equations through successive partial differentiation of the kinetic and potential energies. The equations of motion are coupled in the stiffness matrix and the force vector as a result of the presence of misalignment. The equations of motion are put in dimensionless form for the general situation. The equations of motion for the lateral degrees of freedom are transformed to the complex domain to be solved for dimensionless frequency response. The frequency response revealed that the natural frequencies are excited due to parallel misalignment. The dimensionless transient response of the complete model is solved using Newmark beta and Newton–Raphson methods with small dimensionless time increments to assure capturing all transient dynamic changes. The lateral and torsional natural frequencies are excited during transient and steady state conditions. The steady state spectra reveal that the $1\times$-running speed exciting-component and natural frequencies are present in the translational and rotational degrees of freedom. Finally, the proposed approach of modelling parallel misalignment can be extended to include the effect of angular misalignment by introducing the axial degrees of freedom and applying co-ordinate transformation to the equations of motion.

It is interesting that the foregoing study did not provide any evidence of the presence of second-harmonic ($2\times$) response—a characteristic commonly observed in the field in misaligned rotating shaft systems. It should be noted that the two Jeffcott rotors employed in the model were intentionally assumed to have axisymmetric, linear properties to aid in promoting transparency of the system excitation–response relationships.

Of course, in real machines the bearings and sometimes supports may exhibit non-linear effects and coupling or shaft asymmetries are not uncommon. Additionally, coupling kinematics may play a role in the system dynamics. It is, therefore, proposed here that these effects, i.e., system non-linearities, rotating element asymmetries and, in some cases, coupling kinematics are the main sources of superharmonic vibration in misaligned rotor systems. Work is currently underway to model the influence of these parameters on the vibration response of misaligned shafts.

ACKNOWLEDGMENT

The authors acknowledge the support of Saudi ARAMCO, Saudi Arabia.

REFERENCES

1. H. Lorenzen, E. A. Niedermann and W. Wattinger *Proceedings of the* 18*th Turbomachinery Symposium*, *Dallas*, *TX*, *U.S.A.* 101–110. Solid couplings with flexible intermediate shafts for high speed turbo compressor trains.
2. A. S. Sekhar and B. S. Prabhu 1995 *Journal of Sound and Vibration* **185**, 655–671. Effects of coupling misalignment on vibrations of rotating machinery.
3. M. Xu and R. D. Marangoni 1994 *Journal of Sound Vibration* **176**, 663–679. Vibration analysis of a motor-flexible coupling-rotor system subject to misalignment and unbalance. Part I: theoretical model analysis.
4. M. Xu and R. D. Marangoni 1994 *Journal of Sound Vibration* **176**, 681–691. Vibration analysis of a motor-flexible coupling-rotor system subject to misalignment and unbalance. Part I: experimental validation.

5. B. S. PRABHU 1997 *STLE Tribology Transactions* **40**, 235–242. An experimental investigation on the misalignment effects in journal bearings.
6. G. SIMON 1992 *Proceedings of the Institution of Mechanical Engineers*, Vol. 206, 29–39. Prediction of vibration of large turbo-machinery on elastic foundation due to unbalance and coupling misalignment.
7. D. L. DEWELL and L. D. MITHCHELL 1984 *Journal of Vibration, Acoustics, Stress, and Reliability in Design* **106**, 9–16. Detection of a misaligned disk coupling using spectrum analysis.
8. K. W. WATTNER, *Proceedings of the Fourth Turbomachinery Symposium, Texas A&M* 143–148. High speed coupling failure analysis.
9. A. B. PALAZZOLO, S. R. LOCKE, M. CALISTRAT, R. W. CLARK, Jr., A. AYOUB, D. CALISTRAT and P. TANG *Proceedings of the* 21*st Turbomachinery Symposium, Texas A&M* 83–96, Gear coupling misalignment induced forces and their effect on machinery vibration.
10. H. P. BLOCH, *Proceedings of the Fourth Turbomachinery Symposium, Texas A&M* 149–152. Less costly turboequipment uprates through optimized coupling selection.
11. C. B. GIBBSON 1977 *Proceedings of the Fifth Turbomachinery Symposium, Gas Turbine Laboratories, Texas A & M University, College Station, TX*, 111–116 Coupling misalignment forces.
12. J. MANCUSO 1995 *Proceedings of the Fifth Turbomachinery Symposium, Gas Turbine Laboratories, Texas A & M University, College Station, TX*, 167–177. General purpose vs. special purpose couplings.
13. R. M. ROSENBERG 1958 *Journal of Applied Mechanics* **25**, 47–51. On the dynamical behavior of rotating shafts driven by universal (Hooke) coupling.
14. M. SAIGO, Y. OKADA and K. ONO 1997 *Journal of Vibration and Acoustics* **119**, 221–229. Self-excited vibration caused by internal friction in universal joints and its stabilizing method.
15. P. P. SHEU, W. H. CHIENG and A. C. LEE *Journal of Vibrations and Acoustics* **118**, 88–99. Modeling and analysis of the intermediate shaft between two universal joints.
16. J. H. HUDSON *Proceedings of the* 21*st Turbomachinery Symposium, Texas A&M* 113–123. Lateral vibration created by torsional coupling of centrifugal compressor system driven by a current source drive for a variable speed induction motor.
17. B. O. AL-BEDOOR, K. A. MOUSTAFA and K. M. AL-HUSSAIN 1999 *Journal of Sound and Vibration* **220**, 729–748. Dual dynamic absorbers for the torsional vibrations of synchronous motor-driven compressor.
18. J. R. MANCUSO, C. B. GIBBONS and R. E. MUNYON 1990 *Proceeding of the Eighth Turbomachinery Symposium, Gas Turbine Laboratories, Texas A & M University, College Station, TX*, 141–164. The application of flexible couplings for turbomachinery.
19. E. J. GUNTER, J. C. NICHOLAS and P. E. ALLAIRE 1996 *Journal of Engineering for Power* **96**, 171–181. Effect of residual shaft bow on unbalance response and balancing of a single mass flexible rotor.

APPENDIX A: NOMENCLATURE

c	damping coeffficient
$[\mathbf{C}]$	damping matrix
$[c^*]$	dimensionless damping matrix
e_1, e_2	imbalance eccentricity
$\{\mathbf{F}\}$	force vector
$\{\mathbf{F}^*\}$	dimensionless force vector
$\mathbf{g}$	gravitational constant
i	$\sqrt{-1}$
J_1, J_2	disk polar moment of inertia
k_1, k_2	shaft support stiffness
k'_1, k'_2	shaft lateral stiffness
k_{t1}, k_{t2}	shaft torsional stiffness
$[\mathbf{k}]$	stiffness matrix
$[\mathbf{k}^*]$	dimensionless stiffness matrix
m_1, m_2	masses of the disks
$[\mathbf{m}]$	inertia matrix
$[\mathbf{m}^*]$	dimensionless inertia matrix

$\{\mathbf{Q}\}$	generalized force vector
$\{\mathbf{q}\}$	generalized spatial co-ordinate
$\{\dot{\mathbf{q}}\}$	generalized velocity co-ordinate
$\{\ddot{q}\}$	generalized acceleration co-ordinate
t	time
t^*	dimensionless time
T	kinetic energy
T_i	input torque
T_i^*	dimensionless input torque
T_L	load torque
T_L^*	dimensionless load torque
V	potential energy
x_a	coupling displacement
x_a^*	dimensionless coupling displacement
x_1, x_2	displacements
x_1^*, x_2^*	dimensionless displacements
$\dot{x}_1$, $\dot{x}_2$	velocities
$\dot{x}_1^*$, $\dot{x}_2^*$	dimensionless velocities
$\ddot{x}_1$, $\ddot{x}_2$	accelerations
$\ddot{x}_1^*$, $\ddot{x}_2^*$	dimensionless accelerations
y_1, y_2	displacements
y_1^*, y_2^*	dimensionless displacement
y_a	coupling displacement
y_a^*	dimensionless coupling displacement
$\dot{y}_1$, $\dot{y}_2$	velocities
$\dot{y}_1^*$, $\dot{y}_2^*$	dimensionless velocities
$\ddot{y}_1$, $\ddot{y}_2$	accelerations
$\ddot{y}_1^*$, $\ddot{y}_2^*$	dimensionless acceleration
z_1^*, z_2^*	dimensionless complex displacements
α	Newmark beta parameter for accuracy and stability
β	Newmark beta parameter for accuracy and stability
β_1, β_2	angular position
$\dot{\beta}_1$, $\dot{\beta}_2$	angular speed
$\dot{\beta}_1^*$, $\dot{\beta}_2^*$	dimensionless angular speed
$\ddot{\beta}_1$, $\ddot{\beta}_2$	angular acceleration
$\ddot{\beta}_1^*$, $\ddot{\beta}_2^*$	dimensionless angular acceleration
φ	coupling angular position
ϕ_{u1}, ϕ_{u2}	imbalance phase angle
ϕ_m	misalignment phase angle
ζ	damping ratio
ε	error criteria
δ	misalignment magnitude